1. If H_F conserves the total isospin, then

$$A(r,\theta)=A(r,-\theta) \tag{64}$$

and

$$B(r,\theta)=0. \tag{65}$$

Furthermore, since the total isospin I of the 3π system must be in the $I=0$ state,

$$A(r,\theta)=\sum_{l=0}^{\infty}\alpha_{3l}(r)\cos 3l\theta. \tag{66}$$

In this case, there is no C-violation effect in the decay of $\omega^0\to 3\pi$.

2. If $I\neq 3$, then

$$\beta_{3l}(r)=-3\alpha_{3l}'(r), \tag{67}$$

where $l=$ any positive integer.

3. If the final state interactions between pions are neglected, then by using the CPT invariance and choosing $\alpha_0(r)$ to be real, we find

$$\alpha_l(r)=\text{real},\quad \alpha_l'(r)=\text{pure imaginary},$$

and

$$\beta_{3l}'(r)=\text{pure imaginary}.$$

Thus, if a charge asymmetry is observed in ω^0 decay, it implies that the C-noninvariant interaction H_F exists, that it does not conserve the isospin, and that the final-state pion interactions cannot be neglected.

For a simple phenomenological analysis, one may assume the final 3π system to be in $I=0$ and $I=1$ states only. The simplest form of $A(r,\theta)$ is given by

$$A(r,\theta)=a+be^{i\phi_b}r\sin\theta, \tag{68}$$

where $a\geqq 0$, $b\geqq 0$ and ϕ_b are three real parameters. The relative amplitudes of the $I=0$ state and the $I=1$ state are given, respectively, by a and b. The phase ϕ_b gives the measure of the relevant final-state interactions, since $\phi_b=\pm\pi/2$ if the final-state interactions are neglected. Assuming that H_F contains a $|\Delta\mathbf{I}|=1$ part, the magnitude of the asymmetry parameter b/a may be estimated to be $\sim(Fm_p^2)\sim 10^{-2}$.

ACKNOWLEDGMENTS

I wish to thank P. Franzini, M. Schwartz, and C. S. Wu for discussions.

PHYSICAL REVIEW VOLUME 139, NUMBER 5B 6 SEPTEMBER 1965

Anti-Isobar Production in $\bar{p}n$ Interactions*

T. C. Bacon, H. W. K. Hopkins, D. K. Robinson, and E. O. Salant
Brookhaven National Laboratory, Upton, Long Island, New York

and

A. Engler, H. E. Fisk, C. M. Meltzer, and J. Westgard
Carnegie Institute of Technology, Pittsburgh, Pennsylvania

(Received 16 April 1965)

Single-pion production in $\bar{p}n$ interactions has been studied in the BNL 20-in. deuterium-filled bubble chamber at an incident $\bar{p}$ momentum of 1.96 GeV/c. Copious production of the $\frac{3}{2},\frac{3}{2}$ anti-isobar was observed. The differential cross section as a function of momentum transfer has a distribution consistent with that predicted by one-pion exchange (OPE). The experimental cross section of 5.1±0.5 mb, however, is about half that predicted by the OPE model of Ferrari and Selleri.

I. INTRODUCTION

In this paper we present results obtained in a study of single-pion production in antiproton-deuteron interactions at 1.96 GeV/c. The purpose of the study was to investigate production and decay of the doubly charged state of the $\frac{3}{2},\frac{3}{2}$ anti-isobar in the reactions

$$\begin{array}{l}\bar{p}+n\to \bar{N}^{*--}+p\\ \qquad\quad\searrow\\ \qquad\quad \bar{p}+\pi^-\end{array} \tag{1}$$

and to compare this with the similar reaction previously studied in pp interactions

$$\begin{array}{l}p+p\to N^{*++}+n\\ \qquad\quad\searrow\\ \qquad\quad p+\pi^+.\end{array} \tag{2}$$

Single-pion production in p-p collisions in the 1.5–4.0-GeV/c momentum region has been the subject of several experimental investigations.[1] Qualitative fea-

* Work performed under the auspices of the U. S. Atomic Energy Commission.

[1] W. J. Fickinger, E. Pickup, D. K. Robinson, and E. O. Salant, Phys. Rev. **125**, 2082 (1962); A. P. Batson, B. B. Culwick, J. G. Hill, and L. Riddiford, Proc. Roy. Soc. (London) **A251**, 218 (1959); G. A. Smith, H. Courant, E. C. Fowler, H. Kraybill, J. Sandweiss, and H. Taft, Phys. Rev. **123**, 2160 (1961).

tures of these experiments were successfully described by the Lindenbaum-Sternheimer isobar model,[2] and by the one-pion-exchange (OPE) isobar model of Selleri.[3] The refinement by Ferrari and Selleri[4] of the OPE model to include form factors and kinematic corrections for off-shell pion-nucleon scattering has been particularly successful in fitting differential and total cross sections over this energy region.

Several experiments on pion production in inelastic $\bar{p}p$ interactions in the 3–4 BeV/c region have been reported.[5,6] The data of the Yale-BNL collaboration[5] on double-pion production through simultaneous isobar-anti-isobar excitation are in good quantitative agreement with an OPE model in which form factors from pp experiments are assumed. Shapes of the momentum-transfer distributions in single-pion production[6,7] are in agreement with the model, but the experimental cross sections are considerably smaller than those predicted. Strong absorptive effects, which are not included in the simple OPE model, may be responsible for the disagreement.

The $\bar{p}n$ interaction (reaction 1) has an initial state of pure isospin ($I=1$), and is particularly convenient for the study of single-pion production in that all particles in the final state are charged. In the OPE model, reactions 1 and 2 have identical isospin properties, as can be seen by comparison of the diagrams of Fig. 1(a) and 1(b). However, since the two initial particles in reaction 2 are identical, there is a second diagram [Fig. 1(d)] leading to the same final state, resulting from interchange of the initial protons. The corresponding diagram [Fig. 1(c)] in reaction 1 leads to the final state $\bar{n}n\pi^-$ which cannot be measured in the present experiment.

Other reactions in $\bar{p}n$ and pp interactions leading to the observed final states are shown in Fig. 1(e), 1(f), 1(g), and 1(h). If all pion production occurs through the ($I=\frac{3}{2}$, $J=\frac{3}{2}$) isobar, the ratio of the process of Fig. 1(e) ($I_z=-\frac{1}{2}$) to that of Fig. 1(a) ($I_z=-\frac{3}{2}$), and of the process of Fig. 1(f) ($I_z=\pm\frac{1}{2}$) to that of Fig. 1(b) ($I_z=+\frac{3}{2}$) is 1:9.

Since the target neutron is part of a deuteron, it has been necessary to test the impulse approximation in the analysis of our events. It has been assumed that the proton from the deuteron does not take part in the reaction, so that the momentum of the neutron before the collision is equal and opposite to the measured momentum of the spectator proton. A careful study has been made to determine the range of momenta for which this assumption is valid. The amount of overlap between the two protons in the final state has also been investigated.

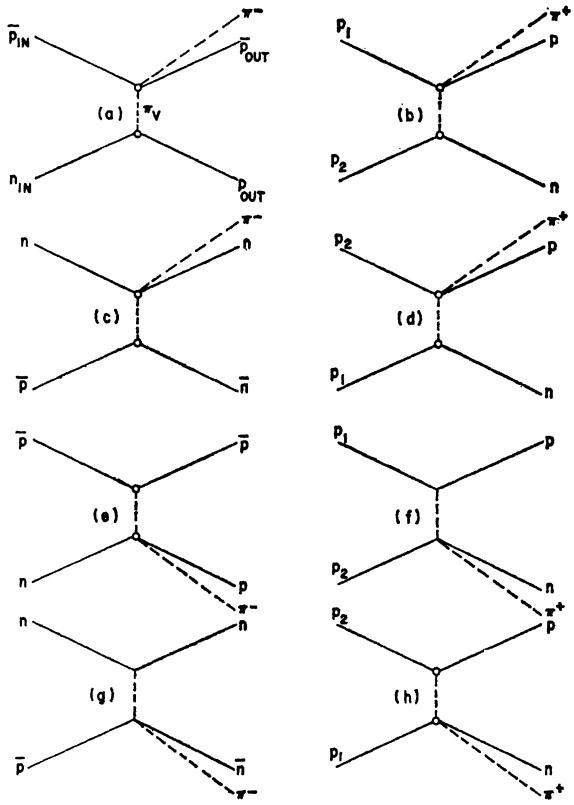

FIG. 1. One-pion-exchange diagrams for single-pion production in pp and $\bar{p}n$ interactions.

Our results are in qualitative agreement with OPE models but our cross section for the reaction $\bar{p}+n\rightarrow\bar{p}+\pi^-+p$ is about half that predicted by Ferrari and Selleri. Recent theoretical treatments[8] which include absorption effects may account for these results.

II. EXPERIMENTAL DETAILS

The Brookhaven National Laboratory 20-in. deuterium-filled bubble chamber was exposed to a separated antiproton beam at the AGS at a momentum of 1.960±0.025 GeV/c. Twenty-five thousand pictures were taken with approximately ten beam tracks per picture. The high quality provided good ionization discrimination between protons and pions. Background particles (π's and μ's) are estimated to be ~2% of the beam.

The pictures were scanned for events within a

[2] R. M. Sternheimer and S. J. Lindenbaum, Phys. Rev. Letters 5, 24 (1960); Phys. Rev. 123, 333 (1961).
[3] F. Selleri, Phys. Rev. Letters 6, 64 (1960).
[4] E. Ferrari and F. Selleri, Nuovo Cimento 27, 1450 (1963).
[5] T. Ferbel, J. Sandweiss, H. D. Taft, M. Gailloud, T. E. Kalogeropoulos, T. W. Morris, and R. M. Lea, Phys. Rev. Letters 9, 351 (1962).
[6] H. C. Dehne, E. Lohrmann, E. Raubold, P. Söding, M. W. Teucher, and G. Wolf, Phys. Rev. 136, B843 (1964).
[7] O. Czyzewski, B. Escoubès, Y. Goldschmidt-Clermont, M. Guinea-Moorhead, T. Hofmokl, D. R. O. Morrison, and S. deUnamuno in *Proceedings of the Sienna International Conference on Elementary Particles, 1963*, edited by G. Bernadini and G. P. Puppi (Società Italiana di Fisica, Bologna, 1963).
[8] K. Gottfried and J. D. Jackson, Nuovo Cimento 33, 309 (1964). L. Durand, III, and Y. T. Chiu, Phys. Rev. Letters 12, 399 (1964), and Phys. Rev. 137, B1530 (1965).

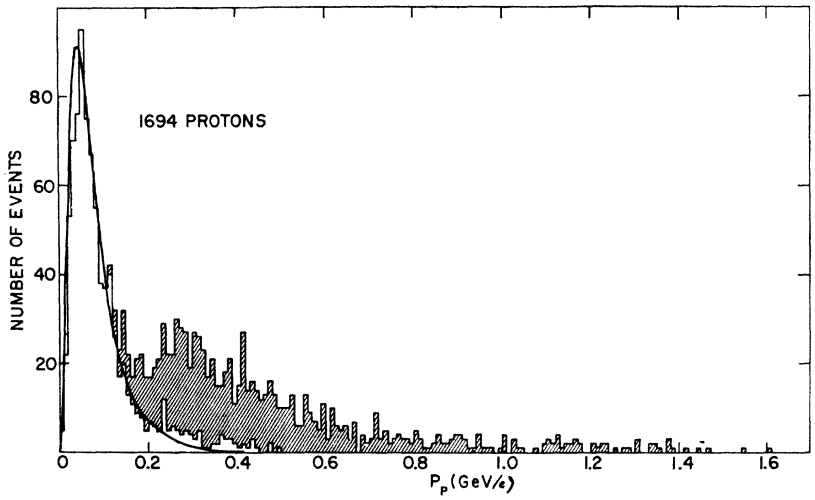

FIG. 2. Distribution of the laboratory momentum P_p of protons from reaction (1). The unshaded region corresponds to the spectator protons.

selected fiducial region which had topologies consistent with the reaction

$$\bar{p}+d\rightarrow\bar{p}+\pi^-+p+p_{\text{spec}}. \tag{3}$$

All three-pronged stars (where the momentum of the spectator proton p_{spec} was insufficient to make a visible track) and those four-pronged stars with one positive track of greater than twice minimum ionization were recorded. These events were measured on digitized projectors and the measurements were analyzed with the TRED-KICK-S.C.F. program on the IBM-7094 computer.

About 40% of the film was rescanned for all three- and four-pronged stars without imposing any ionization criterion. From the two scans an over-all scanning efficiency of approximately 94% was obtained. Events were attributed to the above reaction if: (a) the χ^2 probability for that hypothesis was $\geq 1\%$, and (b) the ionization estimates for the outgoing tracks were in agreement with the kinematic fit.

III. CROSS SECTION

A total of 847 events was attributed to reaction (1), which corresponds to a cross section of 3.92 ± 0.14 mb (based on a deuterium density of 0.137 g/cm^3). To obtain the cross section for the reaction with a free neutron, a correction was applied to take account of the shadowing of the neutron by the proton. The general formalism has been developed by Glauber[9]; for our purpose we have used the calculations of Blair[10] for absorptive $\bar{p}d$ interactions. This correction increases the apparent $\bar{p}n$ cross section by a factor of 1.3. The cross section for the reaction

$$\bar{p}+n\rightarrow\bar{p}+\pi^-+p \tag{4}$$

is thus estimated to be 5.1 ± 0.2 mb. The additional uncertainty in the cross section due to the Glauber correction is about 0.3 mb.

IV. SPECTATOR PROTON

We have defined the proton of lower laboratory momentum to be the "spectator proton." Figure 2 is a histogram of the momenta of both protons. The unshaded region corresponds to the spectator protons. The curve has been computed from the momentum distribution of the proton in the deuteron as predicted by the Hulthén wave function.[11] The agreement is good in the region below about 200 MeV/c; thus, the impulse approximation is considered to be valid in the low-

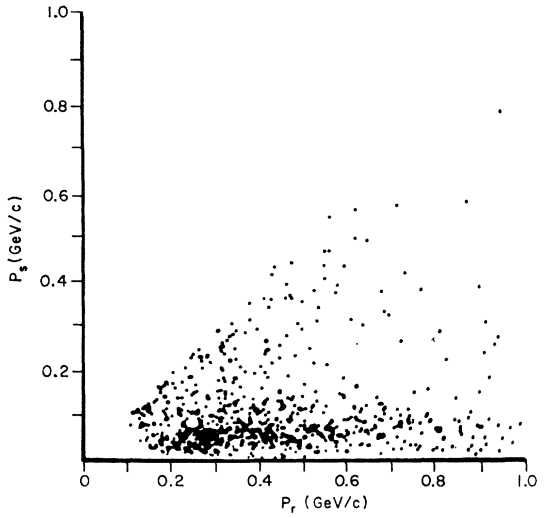

FIG. 3. Scatter plot of spectator-proton momentum (P_s) against recoil-proton momentum (P_r) in the laboratory system.

[9] R. Glauber, Phys. Rev. **100**, 242 (1955).
[10] J. S. Blair, Nucl. Phys. **6**, 348 (1958).
[11] L. Hulthén and M. Sugawara, in *Handbuch der Physik*, edited by S. Flügge (Springer-Verlag, Berlin, 1957), Vol. 39, p. 141.

momentum region. For events in which both protons are in the region of overlap of the two distributions, there is ambiguity in the choice of the spectator.

Figure 3 shows a scatter plot of the momentum of both protons. From the figure we observe that in approximately 10% of the events both protons have momenta less than 200 MeV/c and hence are ambiguous. The depopulation of the region of low proton recoil momentum is a kinematic effect as is evident from Fig. 7. The scatter plot of Fig. 7 shows most of the events concentrated in the region of the isobar. Very small values of q^2 and hence of P_r are kinematically forbidden in this mass region.

It should be noted that the calculations of the $\bar{p}\pi^-$ effective mass and $\bar{p}\pi^-$ scattering angle are independent of the choice of the spectator. In the impulse approximation the square of the four-momentum transfer to the neutron is also independent of that choice. In order that we may consider the neutron as a free target, we shall consider only those events in which the spectator momentum is less than 200 MeV/c in the laboratory system. This limitation restricts the $\bar{p}n$ center-of-mass energies to the range $(2.45_{-0.14}^{+0.18})$ GeV.

V. EFFECTIVE MASS DISTRIBUTIONS AND CHEW-LOW PLOT

Figure 4 shows a Dalitz plot of the square of the $p\pi^-$ and $\bar{p}\pi^-$ invariant masses (M^2). A strong band corresponding to the anti-isobar is clearly visible near $M_{\bar{p}\pi}{}^{-2}=1.5$ (GeV)^2. There is slight evidence here for the $p\pi^-$ isobar. The distributions of the effective masses for the $\bar{p}\pi^-$ and $p\pi^-$ systems are shown in Figs. 5(a) and 5(b). Approximately 75% of the events have effective $\bar{p}\pi^-$ masses between 1160 and 1300 MeV. The $p\pi^-$ mass distribution shows little peaking in the isobar region.

To observe the $\frac{3}{2},\frac{3}{2}$ isobar, it is necessary to eliminate the large background due to the $\bar{p}\pi^-$ anti-isobar. In

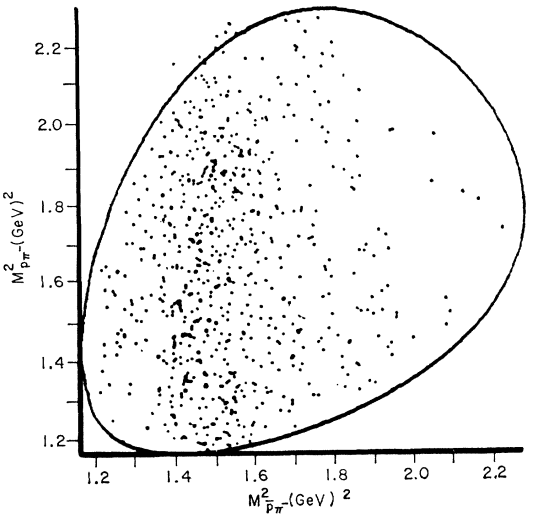

FIG. 4. Dalitz plot of the square of the invariant mass of the $\bar{p}\pi^-$ system against the square of the invariant mass of the $p\pi^-$ system.

Figs. 6(a) and 6(b) the $p\pi^-$ effective mass distributions are plotted for events, respectively outside and inside the $\bar{p}\pi^-$ resonant region (1.16–1.30 GeV). The $p\pi^-$ state is apparent in the selection of events from which the strong $\bar{p}\pi^-$ anti-isobar has been eliminated. Figures 6(c) and 6(d) show effective mass distributions of the $\bar{p}\pi^-$ system for events, respectively, outside and inside the $p\pi^-$ resonant region. Events outside the $p\pi^-$ region show little background.

The effective mass distributions of Figs. 5 and 6 have been fitted to a Breit-Wigner resonance plus phase space background of the form

$$dN=A\times P(m)\times[B+\tfrac{3}{2}\Gamma^2/((m_0-m)^2+\tfrac{1}{4}\Gamma^2)]dm,$$

where dN is the number of events in the interval between m and $m+dm$, $P(m)$ is three-body phase space

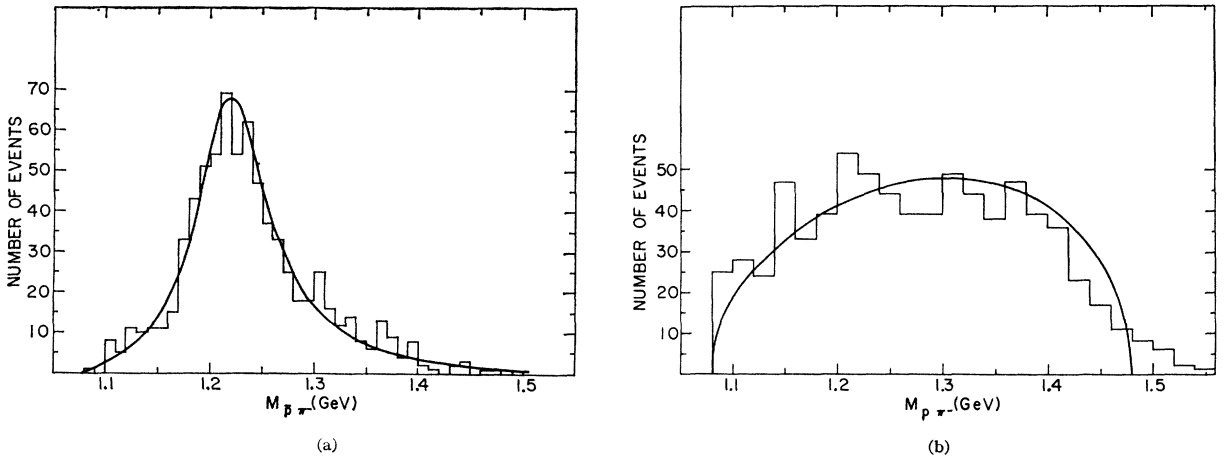

FIG. 5. Invariant mass distribution of (a) the $\bar{p}\pi^-$ and (b) $p\pi^-$ systems. The curve on (a) is a least-squares fit to a Breit-Wigner resonance. The curve on (b) is invariant phase space.

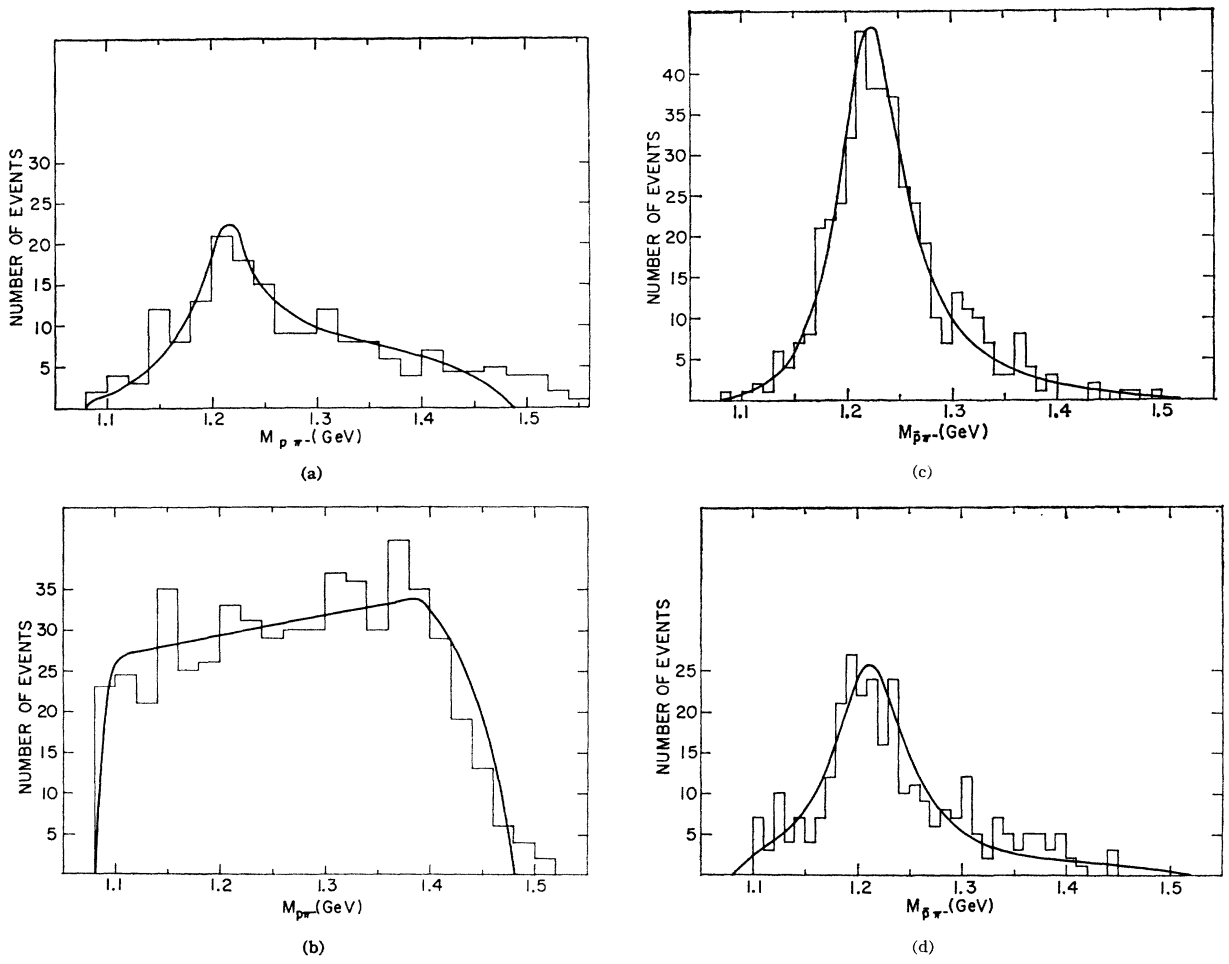

FIG. 6. Invariant mass distributions for (a) the $p\pi^-$ system for events outside the $\bar{p}\pi^-$ resonant region; (b) the $p\pi^-$ system for events inside the $\bar{p}\pi^-$ resonant region; (c) the $\bar{p}\pi^-$ system for events outside the $p\pi^-$ resonant region; and (d) the $\bar{p}\pi^-$ system for events inside the $p\pi^-$ resonant region, where the "resonant region" is defined by $1.16 \leq M_{N\pi} \leq 1.30$ GeV. Figures (a), (c), and (d) have been fitted with a Breit-Wigner resonance distribution with invariant phase space background. The curve on (b) is invariant phase space.

for the event selection considered, and A is a normalizing parameter such that the integral of the function over m gives N, the total number of events in the histogram. Parameters of the fit are B, the constant background term; m_0, the resonance mass; and Γ, the resonance width.

Table I lists the best values of the parameters obtained from the least-squares fitting procedure. (The background is given as a fraction of the total distribution.)

From the distributions of Fig. 6 from which most of the background has been eliminated, the ratio of cross sections for producing the $p\pi^-$ and $\bar{p}\pi^-$ resonance is

$$\sigma(N^*)/\sigma(\bar{N}^*) = 0.139 \pm 0.038$$

consistent with the ratio 1/9, expected for production of the $(I=\frac{3}{2})$ isobar.

It may be noted that the best values of the parameters m_0 and Γ are not in particularly good agreement with the accepted mass and width of the $\frac{3}{2},\frac{3}{2}$ isobar ($m_0 = 1236 \pm 2$ MeV, $\Gamma = 125$ MeV) obtained from πp scattering experiments.[12] However, the mass of the $\frac{3}{2},\frac{3}{2}$ isobar obtained in inelastic-scattering experiments in bubble chambers is generally around 1220 MeV,[1] with which our value for the pure anti-isobar is in good agreement. The width of the isobar as measured in bubble chamber experiments shows wide variation[1] presumably due to strong final-state interactions.

TABLE I. Parameter from least-squares fit to mass distributions of Figs. 5 and 6.

Selection	Figure	m_0 (MeV)	Γ (MeV)	% background
all $\bar{p}\pi^-$	5(a)	1218±3	82±5	negligible
$p\pi^-$ outside $\bar{N}^*$	6(a)	1213±12	61±22	64±10
$\bar{p}\pi^-$ outside N^*	6(c)	1221±3	74±6	negligible
$\bar{p}\pi^-$ inside N^*	6(d)	1213±4	82±12	4±4

[12] A. H. Rosenfeld, A. Barbaro-Galtieri, W. H. Barkas, P. L. Bastien, and J. Kirz, Rev. Mod. Phys. 36, 877 (1964).

Figure 7 shows a Chew-Low plot of $M_{\bar{p}\pi^-}{}^2$ versus q^2, the square of the four-momentum transfer to the $\bar{p}\pi^-$ system. There is a strong clustering of points about the isobar mass at low four-momentum transfer. Similar features have been observed in studies of pion production in p-p and $\bar{p}$-p interactions,[1,6,7] and have been shown to be consistent with a one-pion-exchange (OPE) mechanism for pion production.

VI. MOMENTUM-TRANSFER DISTRIBUTIONS AND THE OPE MODEL

The OPE model of Ferrari and Selleri reproduces remarkably well the features of single-pion production in p-p collisions, between 1–3-BeV incident kinetic energy. On the other hand, Czyzewski *et al.*,[7] the Yale-BNL collaboration,[5] and Dehne *et al.*,[6] have observed a reduction in the cross section for single-pion production in $\bar{p}$-p interactions (a mixture of both isospin 0 and 1 states). In addition, the latter authors found agreement between their $\partial\sigma/\partial q^2$ distributions and the Ferrari-Selleri model for low-momentum transfers. It seems possible that the discrepancy for large values of q^2 could be explained by baryon-antibaryon annihilation in the incoming and outgoing channels.

Figure 8(a) shows our differential cross section as a function of q^2. The curve has been calculated from the equations of Ferrari and Selleri for the OPE diagram of Fig. 1(a). Diagram 1(c) has been neglected since it contributes only about 10% to the production. The calculated differential cross section is considerably larger than the experimental one for all momentum

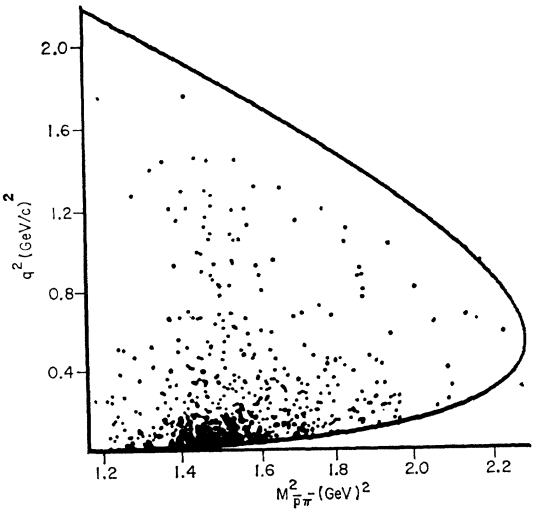

FIG. 7. Chew-Low plot of the square of the invariant mass of the $\bar{p}\pi^-$ system $(M_{\bar{p}\pi^-})^2$ against the four-momentum transfer (q^2).

transfers. Possible interference effects between the two final-state protons have been considered. Such effects are small and confined to the region of low $q^2[q^2<0.05$ $(\mathrm{GeV}/c)^2]$ where the spectator-proton and recoil-proton momenta are similar.

The predicted cross section for reaction (1) is 11 mb, whereas the observed value is 5.1 ± 0.5 mb which includes the uncertainty in the Glauber correction. The situation is similar for the events selected within the isobar peak (1.16 to 1.30 GeV) in Fig. 8(b).

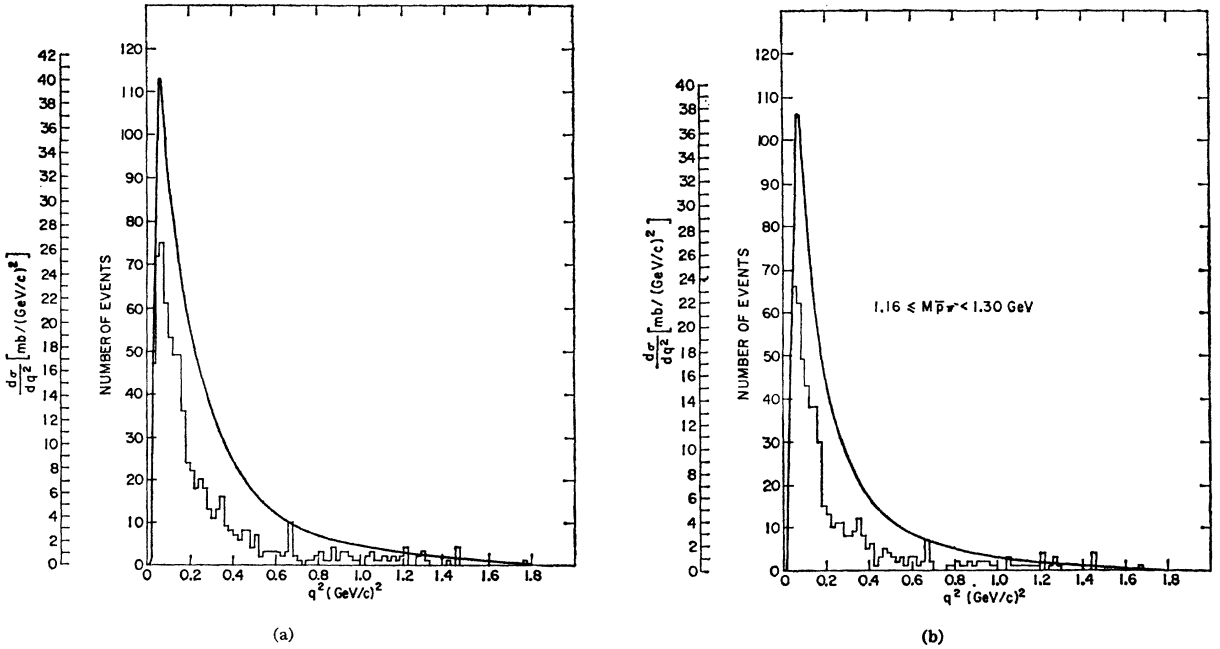

FIG. 8. Experimental differential cross section $d\sigma/dq^2$ compared with the prediction of Ferrari and Selleri for the OPE diagram of Fig. 1(a). (a) All events. (b) Events selected within the $\bar{p}\pi^-$ resonant region $(1.16\leq M_{\bar{p}\pi^-}<1.30$ GeV).

VII. ANGULAR DISTRIBUTIONS

Further information about the importance of the OPE mechanism in isobar production may be obtained from the angular distributions of the isobar decay. The most appropriate angles for this purpose are the pion-nucleon scattering angle (θ) in the isobar rest frame and an azimuthal angle in this system, the Treiman-Yang angle (φ).[13] For production of the $\frac{3}{2},\frac{3}{2}$ isobar by a pure OPE process, the predicted θ angular distribution is the form $1+3\cos^2\theta$ and the φ angular distribution is uniform in φ.[14]

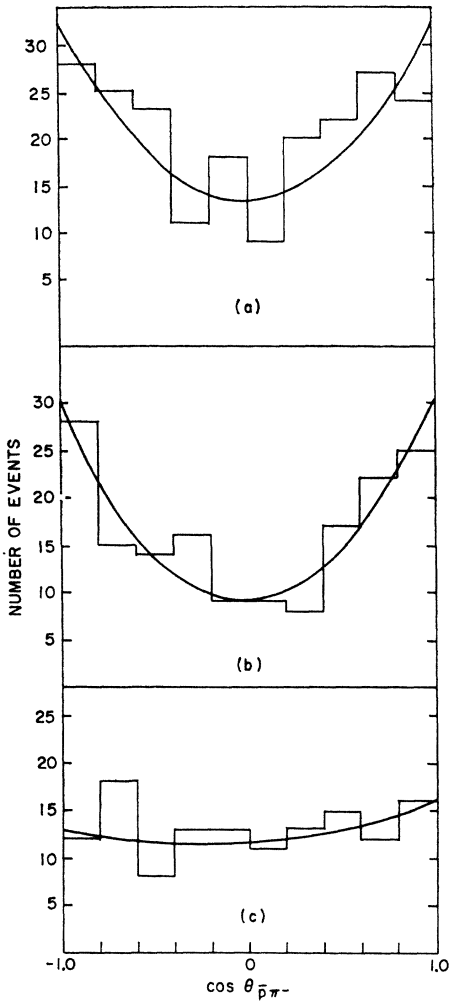

FIG. 9. Distribution of the cosine of the $\bar{p}\pi^-$ scattering angle θ for events with $1.16\leq M_{\bar{p}\pi^-}<1.30$ GeV. (a) $q^2<5M_\pi^2$; (b) $5\leq q^2<10M_\pi^2$; (c) $10\leq q^2<30M_\pi^2$. The curves are least-squares fits to the data of the form $a_0+a_1\cos\theta+a_2\cos^2\theta$.

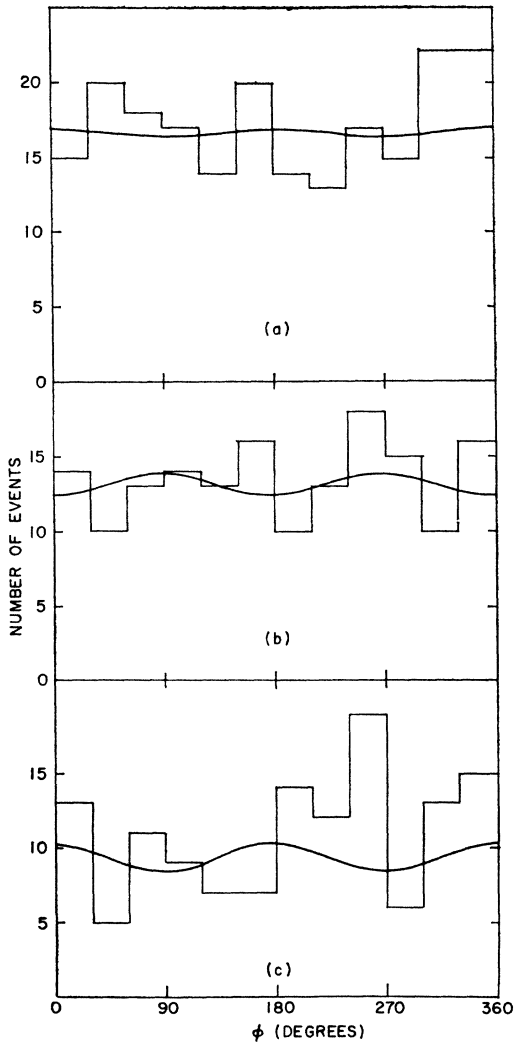

FIG. 10. Distribution of the Treiman-Yang angle φ for events with $1.16\leq M_{\bar{p}\pi^-}<1.30$ GeV. The momentum-transfer regions are the same as those of Fig. 9.

The presence of strong absorption processes in isobar production would modify these simple distributions. Jackson[15] has recently provided predictions in terms of the spin density matrix of the isobars. For reactions (1) and (2) the general decay angular distribution is given by

$$W(\theta,\phi)=(3/4\pi)\{\rho_{33}\sin^2\theta+\rho_{11}(\tfrac{1}{3}+\cos^2\theta)-(2/\sqrt{3})\,\mathrm{Re}\rho_{3,-1}\sin^2\theta\cos2\phi-(2/\sqrt{3})\,\mathrm{Re}\rho_{31}\sin2\theta\cos\phi\}.$$

In this equation ρ_{33}, $\rho_{3,-1}$, and ρ_{31} are elements of the

[13] S. B. Treiman and C. N. Yang, Phys. Rev. Letters 8, 140 (1962). Here $\cos\theta=\hat{\pi}_v\cdot\hat{\pi}^-$ and φ is the angle between the normals to the two planes $\hat{n}_1$ and $\hat{n}_2$, defined by $\hat{\pi}_v\times\mathbf{p}_{\mathrm{out}}$ and $\hat{\pi}_v\times\mathbf{p}_{\mathrm{out}}$, respectively, where all momenta are in the isobar rest frame.

[14] J. Ashkin, J. P. Blaser, F. Feiner, and M. O. Stern, *Proceedings of the CERN Symposium on High-Energy Accelerators and Pion Physics, Geneva, 1956* (European Organization of Nuclear Research, Geneva, 1956), p. 225. The distribution in θ is of the form $1+3\cos^2\theta$ only at the peak of the resonance. Averaged over the rather broad range of effective masses we have used, the angular distribution should be closer to $1+2.5\cos^2\theta$.

[15] J. D. Jackson, Rev. Mod. Phys. 37, 484 (1965).

TABLE II. Coefficients of least-squares fit to scattering angular distributions ($Y=A_0+A_1\cos\theta+A_2\cos^2\theta$) and to the distributions of the Treiman-Yang angle ϕ ($Y=B_0+B_2\cos 2\varphi$). The derived elements of the spin-density matrix are also listed. $\rho_{11}=\frac{3}{4}(A_0+A_2)/(3A_0+A_2)$; $\mathrm{Re}\rho_{3,-1}=\frac{1}{4}\sqrt{3}B_2/B_0$; $\mathrm{Re}\rho_{3,1}=-1.08(\langle\sin 2\theta\cos\varphi\rangle)$.

q^{2a}	A_0	A_1	A_2	B_0	B_2	ρ_{11}	$\mathrm{Re}\rho_{3,-1}$	$\mathrm{Re}\rho_{3,1}$
<5	13.3±1.7	−0.1±2.7	19.4±4.9	16.7±1.2	0.26±1.7	0.41±0.04	−0.01±0.04	−0.02±0.04
5–10	8.9±1.6	0.4±2.4	20.9±4.6	13.1±1.0	−0.7 ±1.5	0.47±0.05	0.02±0.05	0.00±0.04
10–30	11.7±1.7	1.4±2.0	2.8±4.9	9.4±0.8	0.9 ±1.3	0.29±0.05	−0.04±0.06	+0.06±0.05

[a] In units of M_π^2.

matrix, where $\rho_{11}=\frac{1}{2}-\rho_{33}$. For a pure (i.e., nonabsorptive) OPE process, $\rho_{33}=\mathrm{Re}\rho_{3,-1}=\mathrm{Re}\rho_{31}=0$.

For a specific reaction, the ρ's may be predicted from a detailed consideration of the exchange and absorption processes. While predictions have been made for several production processes, there are as yet none available for the reaction considered here. However, examination of the experimental angular distribution and hence, determination of the ρ's should provide useful information about the processes involved.

Figure 9 shows the distribution of the $\bar{p}\pi^-$ scattering angle for $1.16\leq M_{\bar{p}\pi^-}<1.30$ GeV and for three regions of the q^2; $q^2<5m_\pi^2$, $5\leq q^2<10m_\pi^2$, and $q^2\geq 10m_\pi^2$. The effective mass distributions of Figure 6(c) for the $p\pi^-$ system shows that contamination from this state is small within the selected mass region (<5%). Outside this $\bar{p}\pi^-$ mass region, the contamination [Fig. 6(a)] markedly distorts angular distributions.

For $q^2<10M_\pi^2$, the data are within ~2 standard deviations of the expected $1+3\cos^2\theta$. Above $q^2=10M_\pi^2$, the $\cos^2\theta$ term is very weak. The best-fitting curve in the $q^2<10M_\pi^2$ region is $[y=(10.3\pm1.6)-(0.9\pm2.4)\cos\theta+(15.5\pm4.5)\cos^2\theta]$ which is rather weaker than $1+3\cos^2\theta$ expected here.

Figure 10 shows the distribution of the Treiman-Yang angle φ for each q^2 selection. The curves are least-squares fits of the form $a+b\cos 2\varphi$. The distributions for both the $\bar{p}\pi^-$ data and the earlier $p\pi^+$ data[1] are consistent with isotropy.

Finally, we have calculated the values of ρ_{11} and $\mathrm{Re}\rho_{3,-1}$ for the two experiments from the $\cos\theta$ and φ distributions, respectively. The values of $\mathrm{Re}\rho_{31}$ have been obtained by calculating the average value of $\sin 2\theta\cos\varphi$.

The coefficients obtained from the least-square fits to the angular distribution are listed in Table II, with the derived spin-density matrix elements. For all momentum transfer selection $\mathrm{Re}\rho_{3,-1}$ and $\mathrm{Re}\rho_{3,1}$ are consistent with 0, as expected for a pure OPE process. For $q^2<10M_\pi^2$, ρ_{11} is within ~2 standard deviations of the expected value $\rho_{11}=0.5$, for pure OPE.

VIII. CONCLUSION

Production of $\bar{N}^*$ in $\bar{p}n$ interactions appears to occur mainly through a one-pion-exchange process. However, the cross section is smaller by about a factor of 2 than that predicted by the Selleri-Ferrari OPE model with pion form factors. This is in strong contrast to results obtained in an earlier experiment in pp interactions at 2.8 GeV/c which has been shown to be in good agreement with the Selleri-Ferrari model. It would appear that there is strong absorption occurring in the baryon-antibaryon system, as recently discussed by Jackson and by Durand and Chiu.[8,15]

The angular distributions of the $\bar{N}^*$ decay are in good agreement with those predicted by OPE. It thus seems that the absorption process has very slight effect on these distributions.

ACKNOWLEDGMENTS

We wish to thank the BNL Bubble Chamber Group, members of the AGS staff, and our scanners for their invaluable services. We are indebted to Dr. Franco Selleri for many fruitful discussions concerning the OPE model.